

# Model Bacterial Extracellular Polysaccharide Adsorption onto Silica and Alumina: Quartz Crystal Microbalance with Dissipation Monitoring of Dextran Adsorption

KIDEOK D. KWON,<sup>†,‡</sup> HANS GREEN,<sup>§</sup>  
PATRIK BJÖÖRN,<sup>§</sup> AND  
JAMES D. KUBICKI\*<sup>†,||</sup>

*Department of Geosciences and Earth and Environmental Systems Institute, The Pennsylvania State University, University Park, Pennsylvania 16802, and Q-Sense AB, Redegatan 13, SE-426 77 Västra Frölunda, Sweden*

Quartz crystal microbalance with dissipation monitoring (QCM-D) was used to investigate dextran adsorption to alumina and silica. Sensitive adsorption measurements combined with determination of nanometer-scale polymer conformations demonstrate the utility of this technique for studying biopolymer adsorption. The adsorbed amounts and polymeric structures of dextran were determined on Al<sub>2</sub>O<sub>3</sub> and SiO<sub>2</sub> by real-time monitoring of resonance frequency and energy dissipation changes ( $\Delta f$  and  $\Delta D$ ). After the sample was rinsed, the apparent mass of retained dextran was 83 ng/cm<sup>2</sup> on the alumina surface and 9 ng/cm<sup>2</sup> on the silica surface based on the frequency and energy dissipation changes. The  $\Delta D/\Delta f$  ratios were significantly different on the two surfaces, indicating different conformations of the polymers. On alumina, the ratio changed as adsorption proceeded indicating changes of dextran conformation from the initial to latter adsorption steps. On silica, the ratio did not change during the experiments. Therefore, the dissipation and frequency data suggest significantly different mechanisms of dextran adsorption on alumina and silica surfaces. Molecular dynamics simulations of 12 monomeric units of dextran on a silica slab illustrated that H<sub>2</sub>O molecules lead to loosely bound dextran structure onto the SiO<sub>2</sub> surface, consistent with the observed high-energy dissipation in the QCM-D experiments.

## Introduction

Interaction of extracellular polymeric substances (EPS), mainly secreted by microbes (1), with mineral surfaces is an issue in bacterial adhesion, biofilm formation, mineral dissolution, sediment stabilization, and biomineralization (2–5). Adsorption of EPS to mineral surfaces has environmental significance because the adsorbed EPS can change

physicochemical properties of mineral surfaces and affect interactions with pollutants. EPS are accumulators of chlorinated aromatic hydrocarbons (6) and heavy metals (7, 8). EPS can immobilize Fe from the water column by forming Fe-hydroxide precipitates in acid mine drainage (9). EPS can also enhance mobilization of heavy metals and chlorinated hydrocarbons in soils and aquifers (10–12). Therefore, characterization of polymer adsorption to minerals is necessary to understand the effect of EPS on contaminant distribution in subsurface environments.

One widely used technique to measure polymer adsorption is batch or column isotherm experiments (13, 14), which determine the amounts of polymer adsorbed by comparison of solution concentrations before and after adsorption. Batch experiments can involve significant uncertainties when polymers show low affinity to surfaces because of the low sensitivity on adsorbed mass determination. In low-affinity cases, quartz crystal microbalance (QCM) measurements can be useful. QCM can quantify relatively low levels of adsorption (e.g., ng/cm<sup>2</sup>) with real-time monitoring (see refs 15 and 16 for review). Recently, this QCM technique has been used in environmental studies to detect specific organic compounds mainly due to the high sensitivity on adsorbed mass (17, 18).

In addition to isotherms, information on adsorbed polymer conformations is essential to characterize the interactions of polymers with mineral surfaces, because structural changes of the polymers can affect sorption behaviors of contaminants to the polymer-coated surfaces (19–21). IR spectroscopy has been used to identify responsible functional groups and to obtain structures of polymers interacting with mineral surfaces (14, 22, 23). However, it is difficult to obtain conformations of polymers away from the surface from IR techniques alone. Furthermore, IR spectroscopy often needs concentrated samples to achieve significant signal-to-noise ratios.

QCM with dissipation monitoring (QCM-D) can provide information on conformational changes of polymers as well as the mass above the solid/water interface (24). QCM-D has been used to characterize thicknesses (25), conformational changes (26), and water content of polymer films adsorbed to surfaces (27). The surfaces used in biochemistry studies have been mostly gold, TiO<sub>2</sub>, or methyl-terminated surfaces rather than the oxide surfaces that are commonly found in the subsurface environments. In this study, the sensor crystal electrodes were coated with Al<sub>2</sub>O<sub>3</sub> and SiO<sub>2</sub> oxide films to approximate mineral surfaces.

The goals of this study were to examine kinetics of dextran sorption/desorption and to characterize the structure of the adsorbed polymer films on alumina and silica surfaces using QCM-D. The interpretation of the dextran-silica system was complemented with molecular dynamics (MD) simulations. Nearly uncharged dextran (a polysaccharide consisting mainly of glucose 1,6- $\alpha$ -linkages) was chosen as a starting model for an EPS component as it is an important extracellular microbial polysaccharide (28). Because this neutral polysaccharide is known to form weak interactions with silica surfaces (14, 29), a relatively small amount of adsorption is expected as a test of the sensitivity of the QCM-D technology.

## Materials and Methods

**QCM-D Experiments.** QCM-D technology is described elsewhere (30). The general QCM principle is to apply an AC voltage in the MHz range across an AT-cut piezoelectric quartz crystal and to record the resonance frequency of the crystal. In QCM-D, the AC voltage is pulsed to monitor the damping or “ring-down” of the crystal oscillation.

\* Corresponding author phone: (814)865-3951; fax: (814)863-7823; e-mail: kubicki@geosc.psu.edu.

<sup>†</sup> Department of Geosciences, The Pennsylvania State University.

<sup>‡</sup> Current address: Geochemistry Department, Division of Earth Sciences, Mail Stop 90/1116, Lawrence Berkeley National Laboratory, Berkeley, CA 94720.

<sup>§</sup> Q-Sense AB.

<sup>||</sup> Earth and Environmental Systems Institute, The Pennsylvania State University.

QCM is traditionally used to determine the mass adsorbed onto an oscillating quartz crystal with a linear relationship of adsorbed mass ( $\Delta m$ ) of a material with resonance frequency change ( $\Delta f$ ) of the crystal, normally referred to as the Sauerbrey equation (31),

$$\Delta m = -\frac{C_{\text{QCM}}}{n} \Delta f \quad (1)$$

where  $C_{\text{QCM}}$  is the mass sensitivity constant (17.7 ng/cm<sup>2</sup>/Hz at  $f = 5$  MHz),  $n$  is the overtone number (1, 3, 5, ...). On the basis of this relationship, a decreasing resonance frequency corresponds to a proportional mass uptake on the sensor crystal surface. The conditions for this relationship to be valid are as follows:

(i) the adsorbed mass is evenly distributed on the crystal, and  
(ii) the mass is much smaller than the crystal mass itself, and

(iii) the mass is rigid enough not to deform during the crystal oscillation.

Thus, for soft and viscoelastic materials, the linear relationship between frequency and mass is not necessarily valid (32–36) because the materials do not fully couple to the crystal oscillations.

From the decay of the crystal oscillations in a QCM-D experiment, the energy dissipation ( $D$ , dissipation factor) is simultaneously monitored to obtain viscoelastic properties of the material by

$$D = \frac{E_{\text{dissipated}}}{2\pi E_{\text{stored}}} \quad (2)$$

where  $E_{\text{dissipated}}$  is the energy lost during one oscillation, and  $E_{\text{stored}}$  is the energy stored in the oscillating circuit. More dissipation to a material occurs when the adsorbed material deforms during oscillation. Soft materials adsorbed on a crystal surface give a higher  $D$  factor, whereas rigid materials produce a lower  $D$  factor.

Beyond the limitation of the Sauerbrey equation (eq 1), the Voigt-based viscoelastic model (34–35) has been used to obtain more accurate adsorbed mass. In the Voigt-based model,  $\Delta f$  and  $\Delta D$  are related to physical parameters of an adsorbed film (thickness, viscosity, shear modulus, and density). Hence, the viscoelastic parameters and mass of the adsorbed film can be determined by fitting with the simultaneously measured  $\Delta f$  and  $\Delta D$  at multiple overtones.

The  $\Delta D/\Delta f$  ratio gives information on how much energy is dissipated by a material for a unit change in the frequency (26). For example, a high  $\Delta D/\Delta f$  ratio corresponds to a relatively nonrigid open structure, whereas a low ratio corresponds to a stiffer, more compact structure where the adsorbed mass induces relatively low-energy dissipation. In this study, use of the Voigt-based viscoelastic modeling to estimate the adsorbed effective dextran mass is justified because the  $\Delta D/\Delta f$  ratio was relatively high.

Vapor deposited Al<sub>2</sub>O<sub>3</sub> and sputtered SiO<sub>2</sub> onto 5 MHz AT-cut quartz sensor crystals (14 mm diameter disks; Q-Sense, Gothenburg, Sweden) were used to represent two different mineral surfaces. Both surfaces were verified to have the correct composition by X-ray photoelectron spectroscopy (XPS) and the Al<sub>2</sub>O<sub>3</sub> with time-of-flight–secondary ion mass spectrometry as well. The structures of these vapor-deposited films were not and unlikely to be equivalent to  $\alpha$ -quartz or  $\alpha$ -Al<sub>2</sub>O<sub>3</sub>; hence, we contrast adsorption data based solely on composition. The SiO<sub>2</sub>-coated crystals were cleaned in sodium dodecyl sulfate (4%) for 30 min. Crystals coated with Al<sub>2</sub>O<sub>3</sub> were sonicated in ethanol for 15 min. Both surfaces were exposed to UV/ozone treatment for 10 min to ensure full oxidation. Dextran (MW ~ 66.7 kDa Sigma Aldrich D-4751) was diluted in 10 mM NaCl to a series of concentrations at

ca. pH 6 (not buffered to avoid signal interference via adsorption of the buffer): approximately 10, 20, 50, and 100 (6.67 mg/mL)  $\mu$ M.

The QCM-D experiments were conducted with the Q-Sense D300 (Q-Sense, Gothenburg, Sweden) and the QAFC 302 Axial Flow Chamber (Q-Sense, Gothenburg, Sweden) at 22 °C coupled to a peristaltic pump, using 100  $\mu$ L/min flow. When the adsorption of dextran reached saturation at a particular concentration of the polymer, the higher concentration of dextran was successively flowed over the coated sensor crystals. When the highest concentration dextran (100  $\mu$ M) reached saturation, the surfaces were rinsed with 10 mM NaCl solution (pH ~ 6).

Frequency and dissipation changes at the fundamental frequency and three overtone harmonics ( $n = 3, 5,$  and  $7$  at 15, 25, and 35 MHz, respectively) were simultaneously monitored. The data points were sampled at a rate of approximately 50 Hz but were averaged to obtain one data point per resonant frequency per second. The adsorbed mass was estimated with the viscoelastic model (34,35). The software Q-Tools (Q-Sense, Gothenburg, Sweden) was used to analyze the data.

**Molecular Dynamics.** A model SiO<sub>2</sub> surface was generated by cleaving the (0001) surface of  $\alpha$ -quartz from the experimental coordinates using the Surface Builder module of Cerius<sup>2</sup> (Accelrys Inc., San Diego, CA). Hydrogen atoms were added to satisfy the valence of the surface oxygen atoms and to create an electrostatically neutral slab of  $30 \times 30 \times 12 \text{ \AA}^3$ . This surface should be similar to real SiO<sub>2</sub> surfaces in solution because a recent XPS study on quartz surfaces has shown that the predominant surface species of quartz is neutral  $\equiv\text{Si}-\text{OH}$  in ambient solution pH (37). However, the SiOH density of this surface is higher than the observed values.

A dextran molecule of 12 monomeric units was built using Cerius<sup>2</sup> (Accelrys Inc., San Diego, CA) based on the known structure (1,6- $\alpha$ -linkage glucose) and energy minimized in the gas phase with the COMPASS force field (38).

MD simulations were performed using Cerius<sup>2</sup> (Accelrys Inc.). MD simulations on the dextran in the gas phase were performed for 10 ps ( $10^{-12}$  sec) to obtain a structure that was juxtaposed onto the model silica surface. To investigate the role of water in the interactions between dextran and the silica surface, 877 H<sub>2</sub>O molecules were added on top of the dextran/SiO<sub>2</sub> model from a box of  $27 \times 27 \times 40 \text{ \AA}^3$ . The distance between the bottom of the H<sub>2</sub>O box and the top of the SiO<sub>2</sub> model was approximately 10  $\text{\AA}$ . The positions of the all atoms of the model silica surface were fixed, and nonperiodic boundary conditions were used to speed up the simulation process and allow for the maximum number of steps. A time step of 1 fs ( $10^{-15}$  sec) and the Nosé–Hoover thermostat (39) with 300K temperature were used in the NVT MD simulations using the COMPASS force field. The total length of the simulation was 1 ns ( $10^{-9}$  sec, 1 million time steps).

## Results

**Measured Frequency ( $f(t)$ ) Data.** The patterns of the frequency change ( $\Delta f$ ) with time on both surfaces were similar (Figure 1). When higher concentrations of dextran were injected sequentially, the resonance frequency continued to decrease. Near steady-state  $\Delta f$  values for each concentration were reached within approximately 10–20 min. Rinsing the surfaces with 10 mM NaCl solution significantly increased the resonance frequencies.

The magnitude and kinetics of the  $\Delta f$  values were different on the two surfaces, especially in the initial phases of adsorption and rinsing. At the concentration 10  $\mu$ M, the frequency changed by  $-3.0$  Hz on the Al<sub>2</sub>O<sub>3</sub> surface and  $-0.5$  Hz on the SiO<sub>2</sub> surface within 5 min. In the rinsing steps, the Al<sub>2</sub>O<sub>3</sub> surface had a slower desorption rate than the SiO<sub>2</sub>

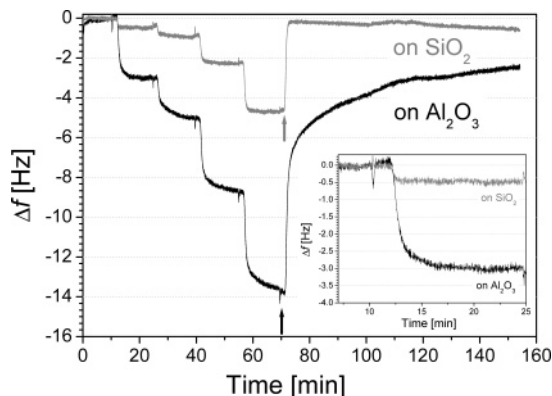


**FIGURE 1.** Frequency changes ( $\Delta f$ ) with time on  $\text{Al}_2\text{O}_3$  and  $\text{SiO}_2$  surfaces. The black line is for dextran on the  $\text{Al}_2\text{O}_3$  surface, and the gray line is for dextran on the  $\text{SiO}_2$  surface. The small peak in the end of each plateau of  $\Delta f$  corresponds to an injection of different concentration solution of dextran (10, 20, 50, and 100  $\mu\text{M}$ ). Arrows indicate the start of surface rinsing. Inset:  $\Delta f$  with time during the first adsorption steps on the two surfaces.

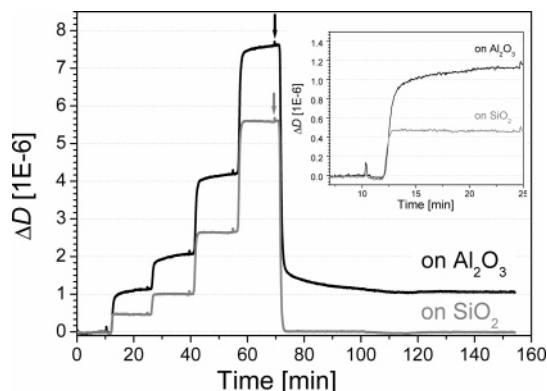


**FIGURE 2.** Dissipation change ( $\Delta D$ ) with time on  $\text{Al}_2\text{O}_3$  and  $\text{SiO}_2$  surfaces. The black line is for dextran on the  $\text{Al}_2\text{O}_3$  surface, and the gray line is for dextran on the  $\text{SiO}_2$  surface. Arrows indicate the start of surface rinsing. Inset:  $\Delta D$  with time during the first adsorption step on the two surfaces.

surface: the frequency leveled out on  $-2.5$  Hz for the  $\text{Al}_2\text{O}_3$  surface after 85 min of rinsing, whereas the frequency returned to  $-0.5$  Hz after 3 min of rinsing for the  $\text{SiO}_2$  surface. At the  $100 \mu\text{M}$  concentration,  $\Delta f$  was  $-13.4$  Hz for the alumina and  $-4.7$  Hz for the silica surfaces.

**Measured Dissipation ( $D(t)$ ) Data.** The time-resolved behaviors of the dissipation ( $D$ ) factor of both surfaces were similar (Figure 2). The  $D$  factor increased rapidly with each injection of higher concentration and reached a saturation stage. However, the dissipation on the alumina surface was higher than on the silica surface during each adsorption step. No residual dissipation change ( $\Delta D$ ) was observed on the silica surface after rinsing, but the alumina surface showed a residual  $\Delta D$  of approximately  $1 \times 10^{-6}$  after the 85 min rinsing.

**$\Delta D$  vs  $\Delta f$  Plots.** Comparison of  $\Delta D$  and  $\Delta f$  data can provide insight to understand the differences in adsorption behaviors such as structural developments during adsorption (26). The plots of  $\Delta D$  against  $\Delta f$  showed different patterns between the two surfaces both in shape and in terms of the  $\Delta D/\Delta f$  ratio (Figure 3). Several regimes with different  $\Delta D/\Delta f$  slopes were observed on the  $\text{Al}_2\text{O}_3$  surface, whereas one  $\Delta D/\Delta f$  slope was observed on the  $\text{SiO}_2$  surface. In addition, the  $\Delta D/\Delta f$  slope for the silica surface was steeper than the ones observed for the alumina surface during adsorption.

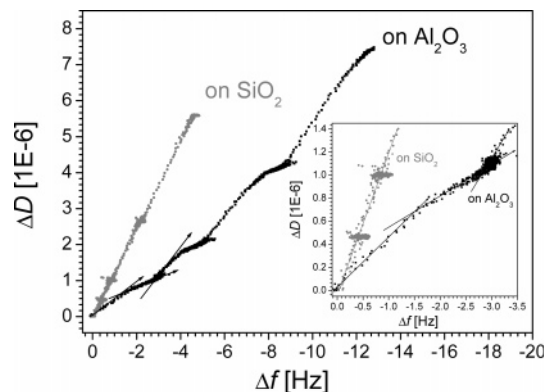


**FIGURE 3.** Plots of  $\Delta D$  versus  $\Delta f$  of adsorbed dextran on two surfaces. The black line is for dextran on the  $\text{Al}_2\text{O}_3$  surface, and the gray line is for dextran on the  $\text{SiO}_2$  surface. Arrow lines guide changes of the  $\Delta D/\Delta f$  ratio during adsorption on the  $\text{Al}_2\text{O}_3$  surface. Inset:  $\Delta D$  versus  $\Delta f$  during the first adsorption step on the two surfaces.

The  $\Delta D/\Delta f$  ratio on the  $\text{Al}_2\text{O}_3$  surface can be divided into at least two regimes during the initial adsorption step using  $10 \mu\text{M}$  dextran (from  $\Delta f = 0$  to  $-3.0$  Hz): a slope with high ratio and a plateau with lower ratio (Figure 3). For subsequent additions of dextran to the  $\text{Al}_2\text{O}_3$  surface, the  $\Delta D/\Delta f$  ratio increased after the plateau and became approximately the same as the slope of  $\Delta D/\Delta f$  ratio for the silica surface.

## Discussion

**Adsorbed Amount of Dextran.** The response to the adsorbed dextran showed the high sensitivity of the QCM-D technique and its comparability to existing batch experimental techniques. The effective mass of adsorbed dextran on  $\text{Al}_2\text{O}_3$  was estimated using the viscoelastic model (34,35) for the QCM-D as  $112 \text{ ng/cm}^2$  after the first adsorption step and  $775 \text{ ng/cm}^2$  at the highest concentration used in this study. For  $\text{SiO}_2$ , the adsorbed mass was  $39 \text{ ng/cm}^2$  after the initial adsorption step and  $550 \text{ ng/cm}^2$  at the last adsorption step before rinse. The residual dextran after final rinsing was estimated to be  $83 \text{ ng/cm}^2$  on the  $\text{Al}_2\text{O}_3$  surface and  $9 \text{ ng/cm}^2$  on the  $\text{SiO}_2$  surface. Previous batch adsorption experiments (14) reported that maximum surface coverage of dextran (MW 80 kDa) was approximately  $28 \text{ ng/cm}^2$  on  $\text{Al}_2\text{O}_3$  particles (BET surface  $100 \text{ m}^2/\text{g}$ ), but the coverage on  $\text{SiO}_2$  particles was below the detection limit.

Use of the Sauerbrey equation (eq 1) for the last adsorption step would predict that the mass was 3.1 times lower for the  $\text{Al}_2\text{O}_3$  surface ( $245 \text{ ng/cm}^2$  instead of  $775 \text{ ng/cm}^2$ ) and 6.6 times lower for the  $\text{SiO}_2$ . This is a large deviation from the Sauerbrey equation but is reasonable as the  $\Delta D/\Delta f$  ratio is high for these two cases. The difference between the two surfaces is also reasonable as this ratio was higher for  $\text{SiO}_2$  than for  $\text{Al}_2\text{O}_3$ , indicating that the film is softer and should therefore cause a larger deviation from the Sauerbrey equation. This example highlights the importance of using a viscoelastic model when quantifying hydrated macromolecular thin films when using QCM-D.

The higher uptake of dextran in the QCM-D experiments compared to the batch experiments can be attributed to water adsorbed and trapped inside dextran on an oscillating sensor crystal. Note that the mass of adsorbed dextran in QCM-D experiments corresponds to polymer adsorbed onto surfaces plus water coupled to the adsorbed polymer. Because all mass coupled to the oscillation of the crystal will be detected as a change of the resonance frequency, the  $\Delta f$  includes bound or trapped liquid molecules within the adsorbed film/material when one side of the oscillating sensor crystal is

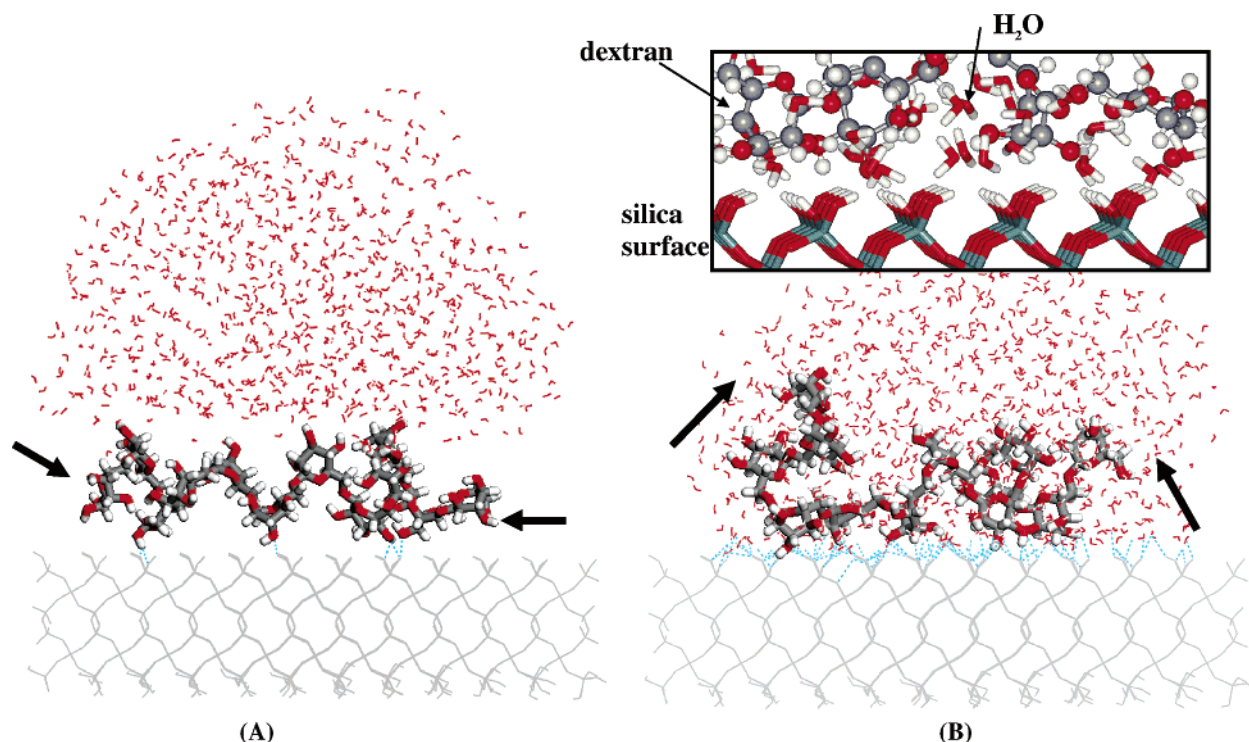


**FIGURE 4.** MD simulation snapshots (A) at 10 ps and (B) at 1 ns. For visualization purposes, the gray network represents a model SiO<sub>2</sub> slab, and small curved rods represent H<sub>2</sub>O molecules. Note that solid arrows indicate tails of dextran takes off the surface. Small dotted lines show possible H-bonds on the surface. Inset: a closer look of interactions on the surface.

immersed in liquid media (36, 40). For example, the H<sub>2</sub>O molecules surrounding the dextran model in Figure 4 (at the 1 ns simulation time) would contribute to the  $\Delta f$ . Thus, the mass obtained by a QCM crystal immersed in liquid is “effective mass” rather than a mass of only the adsorbed polymers, which is generally obtained by batch adsorption experiments and optical techniques such as ellipsometry. This effective mass of adsorbed film including water has been shown to up to 20 times higher (corresponding to 95% water content in the film) than the molar mass of the molecules forming the film (ref 36 and references therein).

The higher adsorption of dextran on alumina compared to silica may be attributed to the difference in hydroxyl group density on mineral surfaces as well as the difference in interaction strengths of hydroxyl groups between dextran and mineral surfaces associated with water molecules. Differences in the adsorption amount of organic compounds on hematite and kaolinite in batch adsorption experiments have been explained by the difference in distribution of hydroxyl groups on the mineral surfaces associated with ionic strength (19); and secondary ion mass spectrometry study has shown that density of surface hydroxyl groups is a major factor in determining adsorption of organic compounds to coated metal-oxides surface (41). The trends that mineral surfaces with high isoelectric point tend to adsorb more polysaccharides than quartz has been explained by the relative difference in acid/base interaction strength between hydroxyl groups (42).

**Conformational Changes During Adsorption.** The plot of  $\Delta D$  versus  $\Delta f$  (Figure 3) shows that the energy dissipation patterns during the initial adsorption step were different between the alumina- and silica-coated crystals for the same amount of dextran introduced. The dissipation shifts ( $\Delta D$ ) were different by up to a factor of 2 between the surfaces throughout the measurements, whereas the frequency shifts ( $\Delta f$ ) differed by up to 6 times during the initial steps. These differences imply that the interactions and conformations of

dextran are different on the Al<sub>2</sub>O<sub>3</sub> surface compared to the SiO<sub>2</sub> surface.

The constant silica  $\Delta D/\Delta f$  ratio (Figure 3) indicates that the viscoelastic properties of dextran were independent of the concentration. Dextran adsorbed to silica in a single-phase manner where the interactions between the dextran and the silica surface were similar to dextran–dextran interactions. Therefore, the silica surface is hypothesized to not change dextran conformation significantly from the conformation taken in solution.

The overall gradual increase of the  $\Delta D/\Delta f$  ratio on the Al<sub>2</sub>O<sub>3</sub> surface (Figure 3) indicates that the alumina surface affected dextran conformations and led to conformational changes during adsorption. The increase of the  $\Delta D/\Delta f$  ratio as adsorption proceeded can be interpreted as dextran settled down in a relatively packed structure during the first step followed by adsorption of more viscous and loose dextran layers. In the later adsorption steps after  $\Delta f = -3.0$  Hz, the  $\Delta D/\Delta f$  increased to the high ratio on the SiO<sub>2</sub> surface. This indicates that the viscoelastic properties of dextran on the alumina surface during the later adsorption steps were similar to the properties of dextran interacting with silica surfaces, implying that the effect of the surface was not as significant as during the initial adsorption step.

The decrease of the  $\Delta D/\Delta f$  ratio for the  $\Delta f = -1.5$  Hz to  $\Delta f = -3.0$  Hz range on the Al<sub>2</sub>O<sub>3</sub> surface (Figure 3) revealed that dextran experienced at least two different adsorption processes on the alumina surface during the initial adsorption phase. The higher  $\Delta D/\Delta f$  ratio from  $\Delta f = 0$  Hz to  $\Delta f = -1.5$  Hz corresponds to dextran adsorption with nonrigid and open structures. Then, the lowering ratio relates to more rigid and compact structure due to more individual dextran attachments to the alumina surface.

**Description of Conformations.** Structures of polymers (e.g., polyelectrolytes) adsorbed onto surfaces have been described with relative positions of polymer segments from the surfaces (e.g., trains, loops, and tails) (43–45), and the

loops are mostly responsible for mass of polymers covered on surface (44). On the basis of this description, dextran on the alumina surface would have a greater number of loops, and dextran on the silica surface would be relatively flat with fewer loops and longer tails, which trap more H<sub>2</sub>O molecules on the silica surface.

**MD Simulations.** Polysaccharides are generally regarded to interact with silica surfaces mainly via H-bonding (14, 42, 46). H<sub>2</sub>O molecules, however, can interfere with the H-bonding of dextran to the silica surface and lead to a loosely bound structure. The H<sub>2</sub>O–silica H-bonding may cause fewer H-bonds to form between dextran and silica. Therefore, during the initial adsorption stage dextran carries many H<sub>2</sub>O molecules inside its structure, and H<sub>2</sub>O molecules occupy most H-bonding sites on the silica surface. This explanation was tested with MD simulations.

The MD simulations were begun with dextran in contact with the silica surface. As the simulation started, the H<sub>2</sub>O molecules moved down and hydrated the dextran model. Some of the H<sub>2</sub>O molecules began to interact with silica surface after approximately 50 ps. The MD simulations at 1 ns showed H<sub>2</sub>O molecules were widely distributed within the dextran model and between the dextran and silica surface models (Figure 4). H<sub>2</sub>O molecules made the end portions of the dextran model detach from the surface and protrude into the surrounding water droplet.

The simulated H<sub>2</sub>O behavior at the interface is similar to results of a recent neutron reflectivity study, in which water absorption by hydrophilic polymers on silicon wafers exposed to a UV ozone (creating a silicon oxide layer) leads to water accumulation at the interface (47). As expected, the dextran model was hydrated with H<sub>2</sub>O molecules, and the silica surface model formed most of the H-bonds with H<sub>2</sub>O molecules rather than with the dextran model.

The use of 12 monomeric units for dextran and 1 ns of simulation are insufficient to completely sample the conformational space of adsorbed dextran. The relaxation time of polymers in QCM is approximately 10–100 ns because the crystal oscillation frequency is in the 10<sup>6</sup>–10<sup>7</sup> Hz range (27), but this length of simulation is impractical for us at this time. Nevertheless, snapshots of the current MD simulations clearly shows that dextran takes a loose and swollen structure due to hydration of H<sub>2</sub>O molecules (Figure 4B) compared to a structure without H<sub>2</sub>O molecules (Figure 4A).

The description of the dextran–silica system by MD simulations is consistent with a previous atomic force microscopy study, in which swelling features of dextran were observed through images and force curves (48). The high content of H<sub>2</sub>O molecules inside the dextran model and the detachment of the dextran tails are consistent with interpretation of the resonance frequency and dissipation data on silica collected in this study.

In summary, this study showed that dextran can have significantly different adsorption and desorption behaviors depending on the mineral surface to which it adsorbs. More dextran adsorbed to the alumina surface than to the silica surface. The desorption rate, time taken for rinsing of dextran until no desorption of dextran is observed, was much slower on the alumina surface than on the silica surface. For similar amounts of dextran adsorbed to each surface, the conformations during the adsorption process continuously changed on the alumina surface, whereas the dextran conformation on the silica surface was constant.

The different adsorption and desorption behaviors of polymers adsorbed to mineral surfaces are likely to have significant effects on the fate of contaminants in soils and groundwater aquifers. In particular, recent X-ray standing wave studies have suggested that chemical properties of organic films are key factors to determine distribution of heavy metals at biofilm/mineral interfaces (49,50). The

current QCM-D study implies that conformations of thin polymer film depending on mineral surfaces would be another important characteristic of biofilms in partitioning of pollutants at the interfaces.

The QCM-D technique is promising in diverse environmental and biogeochemical studies due to its high sensitivity (ng/cm<sup>2</sup>) of adsorbed mass and longer range structural information in real-time in combination with its flexibility with substrate material. For example, slow desorption of organic molecules from soils has been regarded as a rate-limiting step in biodegradation and bioremediation (51). Thus, recognition and characterization of the slow desorption process have been important to help bioremediation plans (52). QCM-D could be useful for slow sorption/desorption kinetic studies of organic materials. Furthermore, a few previous studies have shown the successful application of QCM techniques to adsorption studies of bacteria (53), oxoanions (e.g., phosphate and arsenate (54)), and heavy metal ions (e.g., Pb(II) (55)). Therefore, QCM-D is expected to be a useful technique to study EPS, microbes, natural organic matter, and pollutant interactions with surfaces by complementing other experimental techniques such as batch experiments and IR techniques.

### Acknowledgments

This study was supported by the NSF CRAEMS Grant CHE-0089156 and ACS-PRF 41132-AC2. K.D.K. acknowledges partial support of the Penn State Biogeochemical Research Initiative for Education (BRIE) sponsored by NSF (IGERT) Grant DGE-9972759.

### Literature Cited

- (1) Wingender, J.; Neu, T. R.; Flemming, H.-C. What are bacterial extracellular polymeric substances? In *Microbial extracellular polymeric substances: characterization, structure, and function*; Wingender, J., Neu, T. R., Flemming, H.-C., Eds.; Springer: Berlin, 1999; pp 1–19.
- (2) Fletcher, M. Bacterial attachment in aquatic environments: a diversity of surfaces and adhesion strategies. In *Bacterial Adhesion: Molecular and Ecological Diversity*; Fletcher, M., Ed.; John Wiley & Sons: New York, 1996; pp 1–24.
- (3) Chan, C. S.; De Stasio, G.; Welch, S. A.; Girasole, M.; Frazer, B. H.; Nesterova, M. V.; Fakra, S.; Banfield, J. F. Microbial polysaccharides template assembly of nanocrystal fibers. *Science* **2004**, *303*, 1656–1658.
- (4) Vandevivere, P.; Kirchman, D. L. Attachment stimulates exopolysaccharide synthesis by a bacterium. *Appl. Environ. Microbiol.* **1993**, *59*, 3280–3286.
- (5) Dade, W. B.; Davis, J. D.; Nichols, P. D.; Nowell, A. R. M.; Thistle, D.; Trexler, M. B.; White, D. C. Effects of bacterial exopolymer adhesion on the entrainment of sand. *Geomicrobiol. J.* **1990**, *8*, 1–16.
- (6) Wolfaardt, G. M.; Lawrence, J. R.; Headley, J. V.; Roberts, R. D.; Caldwell, D. E. Microbial exopolymers provide a mechanism for bioaccumulation of contaminants. *Microbiol. Ecol.* **1994**, *27*, 279–291.
- (7) Marqués, A. M.; Bonet, R.; Simonpujol, M. D.; Fuste, M. C.; Congregado, F. Removal of uranium by an exopolysaccharide from *Pseudomonas Sp.* *Appl. Microbiol. Biotechnol.* **1990**, *34*, 429–431.
- (8) Loaec, M.; Olier, R.; Guezennec, J. Uptake of lead, cadmium and zinc by a novel bacterial exopolysaccharide. *Water Res.* **1997**, *31*, 1171–1179.
- (9) Boulton, S.; Johnson, N.; Curtis, C. Recognition of a biofilm at the sediment-water interface of an acid mine drainage-contaminated stream, and its role in controlling iron flux. *Hydrol. Process.* **1997**, *11*, 391–399.
- (10) Chen, J. H.; Lion, L. W.; Ghiorse, W. C.; Shuler, M. L. Mobilization of adsorbed cadmium and lead in aquifer material by bacterial extracellular polymers. *Water Res.* **1995**, *29*, 421–430.
- (11) Jenkins, M. B.; Chen, J. H.; Kadner, D. J.; Lion, L. W. Methanotrophic bacteria and facilitated transport of pollutants in aquifer material. *Appl. Environ. Microbiol.* **1994**, *60*, 3491–3498.
- (12) Nelson, Y. M.; Lion, L. W.; Shuler, M. L.; Ghiorse, W. C. Modeling oligotrophic biofilm formation and lead adsorption to biofilm components. *Environ. Sci. Technol.* **1996**, *30*, 2027–2035.

- (13) Santhiya, D.; Subramanian, S.; Natarajan, K. A. Surface chemical studies on sphalerite and galena using extracellular polysaccharides isolated from *Bacillus polymyxa*. *J. Colloid Interface Sci.* **2002**, *256*, 237–248.
- (14) Jucker, B. A.; Harms, H.; Hug, S. J.; Zehnder, A. J. B. Adsorption of bacterial surface polysaccharides on mineral oxides is mediated by hydrogen bonds. *Colloids Surf., B* **1997**, *9*, 331–343.
- (15) Bizet, K.; Gabrielli, C.; Perrot, H. Biosensors based on piezoelectric transducers. *Analisis* **1999**, *27*, 609–616.
- (16) Buttry, D. A.; Ward, M. D. Measurement of interfacial processes at electrode surfaces with the electrochemical quartz crystal microbalance. *Chem. Rev.* **1992**, *92*, 1355–1379.
- (17) Jimenez, O. A.; Chikneyan, S.; Baca, A. J.; Wang, J. X.; Zhou, F. M. Sensitive detection of sulfhydryl groups in surface-confined metallothioneins and related species via ferrocene-capped gold nanoparticle/streptavidin conjugates. *Environ. Sci. Technol.* **2005**, *39*, 1209–1213.
- (18) Applebee, M. S.; Geissler, J. D.; Schellinger, A. P.; Jaeger, R. J.; Pierce, D. T. Field screening of waterborne petroleum hydrocarbons by thickness shear-mode resonator measurements. *Environ. Sci. Technol.* **2004**, *38*, 234–239.
- (19) Murphy, E. M.; Zachara, J. M.; Smith, S. C.; Phillips, J. L.; Wietsma, T. W. Interaction of hydrophobic organic-compounds with mineral-bound humic substances. *Environ. Sci. Technol.* **1994**, *28*, 1291–1299.
- (20) Myneni, S. C. B.; Brown, J. T.; Martinez, G. A.; Meyer-Ilse, W. Imaging of humic substance macromolecular structures in water and soils. *Science* **1999**, *286*, 1335–1337.
- (21) Weber, W. J.; Huang, W. L.; LeBoeuf, E. J. Geosorbent organic matter and its relationship to the binding and sequestration of organic contaminants. *Colloids Surf., A* **1999**, *151*, 167–179.
- (22) Omoike, A.; Chorover, J.; Kwon, K. D.; Kubicki, J. D. Adhesion of bacterial exopolymers to alpha-FeOOH: Inner-sphere complexation of phosphodiester groups. *Langmuir* **2004**, *20*, 11108–11114.
- (23) Wei, J.; Saxena, A.; Song, B.; Ward, B. B.; Beveridge, T. J.; Myneni, S. C. B. Elucidation of functional groups on gram-positive and gram-negative bacterial surfaces using infrared spectroscopy. *Langmuir* **2004**, *20*, 11433–11442.
- (24) Marx, K. A. Quartz crystal microbalance: A useful tool for studying thin polymer films and complex biomolecular systems at the solution-surface interface. *Biomacromolecules* **2003**, *4*, 1099–1120.
- (25) Vogt, B. D.; Soles, C. L.; Lee, H. J.; Lin, E. K.; Wu, W. L. Moisture absorption and adsorption kinetics in polyelectrolyte films: Influence of film thickness. *Langmuir* **2004**, *20*, 1453–1458.
- (26) Höök, F.; Rodahl, M.; Kasemo, B.; Brzezinski, P. Structural changes in hemoglobin during adsorption to solid surfaces: Effects of pH, ionic strength, and ligand binding. *Proc. Natl. Acad. Sci. U.S.A.* **1998**, *95*, 12271–12276.
- (27) Vörös, J. The density and refractive index of adsorbing protein layers. *Biophys. J.* **2004**, *87*, 553–561.
- (28) Kennedy, J. F.; White, C. A. The plant, algal, and microbial polysaccharides. In *Carbohydrate chemistry*; Kennedy, J. F., Ed.; Oxford University Press: New York, 1988; pp 220–262.
- (29) Baudin, I.; Ricard, A.; Audebert, R. Adsorption of dextrans and pullulans at the silica-water interface; Hydrodynamic layer thickness measurements; Role in the fouling of ultrafiltration membranes. *J. Colloid Interface Sci.* **1990**, *138*, 324–331.
- (30) Rodahl, M.; Hook, F.; Krozer, A.; Brzezinski, P.; Kasemo, B. Quartz-crystal microbalance setup for frequency and Q-factor measurements in gaseous and liquid environments. *Rev. Sci. Instrum.* **1995**, *66*, 3924–3930.
- (31) Sauerbrey, G. Use of quartz oscillators for weighing thin layers and for microweighing. *Z. Phys.* **1959**, *155*, 206–222.
- (32) White, C. C.; Schrag, J. L. Theoretical predictions for the mechanical response of a model quartz crystal microbalance to two viscoelastic media: A thin sample layer and surrounding bath medium. *J. Chem. Phys.* **1999**, *111*, 11192–11206.
- (33) Vogt, B. D.; Lin, E. K.; Wu, W. L.; White, C. C. Effect of film thickness on the validity of the Sauerbrey equation for hydrated polyelectrolyte films. *J. Phys. Chem. B* **2004**, *108*, 12685–12690.
- (34) Domack, A.; Prucker, O.; Rühle, J.; Johannsmann, D. Swelling of a polymer brush probed with a quartz crystal resonator. *Phys. Rev. E* **1997**, *56*, 680–689.
- (35) Voinova, M. V.; Rodahl, M.; Jonson, M.; Kasemo, B. Viscoelastic acoustic response of layered polymer films at fluid-solid interfaces: continuum mechanics approach. *Phys. Scr.* **1999**, *59*, 391–396.
- (36) Höök, F.; Kasemo, B.; Nylander, T.; Fant, C.; Sott, K.; Elwing, H. Variations in coupled water, viscoelastic properties, and film thickness of a Mefp-1 protein film during adsorption and cross-linking: A quartz crystal microbalance with dissipation monitoring, ellipsometry, and surface plasmon resonance study. *Anal. Chem.* **2001**, *73*, 5796–5804.
- (37) Duval, Y.; Mielczarski, J. A.; Pokrovsky, O. S.; Mielczarski, E.; Ehrhardt, J. J. Evidence of the existence of three types of species at the quartz-aqueous solution interface at pH 0–10: XPS surface group quantification and surface complexation modeling. *J. Phys. Chem. B* **2002**, *106*, 2937–2945.
- (38) Sun, H. COMPASS: An ab initio force-field optimized for condensed-phase applications - overview with details on alkane and benzene compounds. *J. Phys. Chem. B* **1998**, *102*, 7338–7364.
- (39) Hoover, W. G. Canonical dynamics: Equilibrium phase-space distributions. *Phys. Rev. A* **1985**, *31*, 1695–1697.
- (40) Fawcett, N. C.; Craven, R. D.; Zhang, P.; Evans, J. A. QCM response to solvated, tethered macromolecules. *Anal. Chem.* **1998**, *70*, 2876–2880.
- (41) Takeda, S.; Fukawa, M.; Hayashi, Y.; Matsumoto, K. Surface OH group adsorption properties of metal oxide films. *Thin Solid Films* **1999**, *339*, 220–224.
- (42) Liu, Q.; Zhang, Y. H.; Laskowski, J. S. The adsorption of polysaccharides onto mineral surfaces: an acid/base interaction. *Int. J. Miner. Process.* **2000**, *60*, 229–245.
- (43) Stumm, W.; Sigg, L.; Sulzberger, B. *Chemistry of the solid-water interface: processes at the mineral-water and particle-water interface in natural systems*; John Wiley & Sons: New York, 1992.
- (44) Norde, W. Driving forces for protein adsorption at solid surfaces. In *Biopolymers at interfaces*; Malmsten, M., Ed.; Marcel Dekker: Inc.: New York, 1998; pp 27–54.
- (45) Foissy, A.; El Attar, A.; Lamarche, J. M. Adsorption of polyacrylic acid on titanium dioxide. *J. Colloid Interface Sci.* **1983**, *96*, 275–287.
- (46) Knözinger, H. Hydrogen bonds in systems of adsorbed molecules. In *The hydrogen bond: recent developments in theory and experiments*; Schuster, P.; Zundel, G.; Sandorfy, C., Eds.; North-Holland Pub. Co.: Amsterdam; New York, 1976; Vol. 3, pp 1263–1364.
- (47) Vogt, B. D.; Soles, C. L.; Jones, R. L.; Wang, C. Y.; Lin, E. K.; Wu, W. L.; Satija, S. K.; Goldfarb, D. L.; Angelopoulos, M. Interfacial effects on moisture absorption in thin polymer films. *Langmuir* **2004**, *20*, 5285–5290.
- (48) Frazier, R. A.; Davies, M. C.; Matthijs, G.; Roberts, C. J.; Schacht, E.; Tendler, S. J. B.; Williams, P. M. High-resolution atomic force microscopy of dextran monolayer hydration. *Langmuir* **1997**, *13*, 4795–4798.
- (49) Templeton, A. S.; Trainor, T. P.; Traina, S. J.; Spormann, A. M.; Brown, G. E. Pb(II) distributions at biofilm-metal oxide interfaces. *Proc. Natl. Acad. Sci. U.S.A.* **2001**, *98*, 11897–11902.
- (50) Yoon, T. H.; Trainor, T. P.; Eng, P. J.; Bargar, J. R.; Brown, G. E. Trace metal ion partitioning at polymer film-metal oxide interfaces: long-period X-ray standing wave study. *Langmuir* **2005**, *21*, 4503–4511.
- (51) Pignatello, J. J.; King, B. S. Mechanisms of slow sorption of organic chemicals to natural particles. *Environ. Sci. Technol.* **1996**, *30*, 1–11.
- (52) Johnson, M. D.; Weber, W. J. Rapid prediction of long-term rates of contaminant desorption from soils and sediments. *Environ. Sci. Technol.* **2001**, *35*, 427–433.
- (53) Rodahl, M.; Höök, F.; Fredriksson, C.; Keller, C. A.; Krozer, A.; Brzezinski, P.; Voinova, M.; Kasemo, B. Simultaneous frequency and dissipation factor QCM measurements of biomolecular adsorption and cell adhesion. *Faraday Discuss.* **1997**, 229–246.
- (54) Iitaka, K.; Tani, Y.; Umezawa, Y. Orthophosphate ion-sensors based on a quartz-crystal microbalance coated with insoluble orthophosphate salts. *Anal. Chim. Acta* **1997**, *338*, 77–87.
- (55) Matsuura, N.; Elliot, D. J.; Furlong, D. N.; Grieser, F. In-situ measurement of lead(II) ion binding to an arachidic acid Langmuir monolayer using a quartz crystal microbalance. *Colloids Surf., A* **1997**, *126*, 189–195.

Received for review July 19, 2006. Revised manuscript received September 22, 2006. Accepted September 28, 2006.

ES061715Q